Author(s): A. Chaudhuri,1 M. Odelius,2 R. G. Jones,3 T.-L. Lee,4 B. Detlefs,5 and D. P. Woodruff1
Article Title: The structure of the Au(111)/methylthiolate interface: New insights from near-edge x-ray absorption spectroscopy and x-ray standing waves
Year of publication: 2009
Link to published version:
http://dx.doi.org/ 10.1063/1.3102095

The structure of the Au(111)/methylthiolate interface: new insights from near-edge X-ray absorption spectroscopy and X-ray standing waves

A. Chaudhuri[1], M. Odelius[2], R.G. Jones[3], T.-L. Lee[4], B. Detlefs[5], D.P.Woodruff[1*]

[1] *Physics Department, University of Warwick, Coventry CV4 7AL, UK*

[2] *Fysikum, AlbaNova University Center, Stockholm University,S-10691 Stockholm, Sweden*

[3] *School of Chemistry, University of Nottingham, Nottingham NG7 2RD, UK*

[4] *Diamond Light Source Ltd, Didcot, Oxfordshire, OX11 0DE,, UK*

[5] *ESRF, BP 220, 38043 Grenoble, Cedex 9, France*

[*] corresponding author, email D.P.Woodruff@warwick.ac.uk

Abstract

The local structure of the Au(111)(√3x√3)R30°-methylthiolate surface phase has been investigated by S K-edge near-edge X-ray absorption fine structure (NEXAFS) both experimentally and theoretically, and by experimental normal-incidence X-ray standing waves (NIXSW) at both the C and S atomic sites. NEXAFS shows not only excitation into the intramolecular σ* S-C resonance, but also into a σ* S-Au orbital perpendicular to the surface, clearly identifying the local S headgroup site as atop an Au atom. Simulations show that it is not possible, however, to distinguish between the two possible adatom reconstruction models; a single thiolate species atop a hollow-site Au adatom, or a dithiolate moiety comprising two thiolate species bonded to a bridge-bonded Au adatom. Within this dithiolate moiety a second σ* S-Au orbital that lies near-parallel to the surface has a higher energy that overlaps that of the σ* S-C resonance. The new NIXSW data show the S-C bond to be tilted by 61° relative to the surface normal, with a preferred azimuthal orientation in <211>, corresponding to the intermolecular nearest-neighbour directions. This azimuthal orientation is consistent with the thiolate being atop a hollow-site Au adatom, but not consistent with the originally-proposed Au-adatom-dithiolate moiety. However, internal conformational changes within this species could, perhaps, render this model also consistent with the experimental data.

1. Introduction

Despite the enormous number of investigations of the 'self-assembled monolayers' (SAMs) formed by n-alkylthiolates, ($CH_3(CH_2)_{n-1}S$-) on Au(111) surfaces (e.g. [1, 2, 3, 4]), due in part to a range of technological applications, the detailed structure of the thiolate/metal interface remains in doubt. Even for the simplest case of methylthiolate, CH_3S-, in a (√3x√3)R30° ordered phase at a coverage of 0.33 ML, there remain fundamental controversies. For the longer alkane chains, the situation is further complicated by the existence of multiple ordered phases; a recent review describes some of the underlying issues and the associated experimental and theoretical evidence [5]. Here we focus on what should be the simplest problem, namely the Au(111)(√3x√3)R30°-CH_3S- system. Until recently, a wide range of theoretical total energy calculations all indicated that the lowest energy structure corresponds to the S head-group atom occupying either a three-fold coordinated hollow site or a two-fold-coordinated bridging site (or some intermediate off-bridge site). By contrast, experimental studies by photoelectron diffraction [6] and normal-incidence X-ray standing waves (NIXSW) [7] identify the local adsorption site to be one-fold coordinated atop. A possible solution to this apparent dilemma has recently emerged through evidence that the Au surface is reconstructed at the interface, with the thiolate species bound to Au adatoms, a possibility not considered in any of the early total energy calculations. There are, however, two conflicting views of the structure of these Au-adatom-thiolate moieties. One model, invoked to explain NIXSW data from a range of different alkythiolate species on Au(111) [8], is that each thiolate bonds atop an Au adatom which itself occupies a hollow site on the surface; for the (√3x√3)R30° phase of adsorbed methylthiolate, these Au adatoms must occupy bulk-continuation sites in the so-called fcc hollows. The second model, derived from scanning tunnelling microscopy (STM) investigations of low coverages of methylthiolate at low temperature [9], is that each Au adatom, which occupies a bridging site on the underlying Au(111) surface, is bound to two thiolate species, one on either side of the adatom, such that the S headgroup atoms are close to atop Au atoms in the underlying surface. In both of these Au adatom models, therefore, the S headgroup atom lies atop an Au atom in a bulk-continuation site, compatible with the NIXSW and photoelectron diffraction data. Density functional theory (DFT) calculations indicate that the Au-adatom-dithiolate moiety is energetically favoured [10], (indeed, the thiolate-atop-an-adatom model was considered and rejected in a much earlier DFT study [11]); however, there is no direct experimental evidence that this species is involved in the (√3x√3)R30°-methylthiolate phase. A recent investigation [12] indicates that surface X-ray diffraction (SXRD) is compatible with partial occupation of these dithiolate species, but the only structural model tested was derived from DFT-based molecular dynamics calculations.

Measurements of near-edge X-ray absorption fine structure (NEXAFS) have been widely used to investigate the orientation of molecular species on surfaces [13]. In this approach the main spectral features seen are identified as excitations from a core level of known symmetry (usually a totally-symmetric *s*-state) into unoccupied molecular orbital states, also referred to as local intra-molecular scattering resonances. The known symmetry of these final-state orbitals, combined with selection rules applied to data recorded in different polarisation directions of the incident radiation, provides the basis of the orientational information. Such a description regards the NEXAFS as an entirely intramolecular phenomenon, with the surface primarily acting as a means of orienting the molecule in space, although energetic shifts in these scattering resonances may be attributable to changes in intramolecular bondlengths induced by the interaction with the substrate. In reality, however, the bonding of a molecule to a surface must introduce new unoccupied molecular orbitals involving substrate atoms or, equivalently, strong electron scattering resonances involving substrate atoms.

Here we show that S K-edge NEXAFS from the Au(111)(√3x√3)R30°-methylthiolate surface is dominated by two features, one attributable to transitions to an intramolecular σ* S-C resonance, the other to a molecule-substrate σ* S-Au resonance. The polarisation angle dependence of this substrate bonding feature provides information on the local interface structure, providing clear identification of local atop bonding. Unfortunately, theoretical calculations show that a further S-Au-adatom resonance present in the dithiolate structure overlaps in energy with the σ* S-C resonance, making it difficult to distinguish the different adatoms models of the basis of the measured NEXAFS spectra.

In addition, however, we also present new data from the normal incidence X-ray standing wave (NIXSW) technique including absorption at both the C and S atoms within the adsorbed methylthiolate. This provides valuable information on the S-C bond orientation in both polar and azimuthal directions relative to the surface, that is potentially capable of distinguishing the different structural models.

2. Experimental and Computational Details

The experimental results presented here were obtained at the European Synchrotron Radiation Facility (ESRF) in Grenoble, France, taking radiation from beamline ID32. The experiments were conducted in an ultra-high vacuum surface science end-station equipped with facilities for *in situ* cleaning and gas dosing, low energy electron diffraction (LEED) to characterise the state of surface long-range order, and a hemispherical electron energy analyser to detect the photoemitted electrons.

The Au(111) sample was cleaned *in situ* by the usual combination of argon ion bombardment and annealing cycles (e.g. [14]) until a clean surface was achieved as indicated by X-ray photoelectron spectroscopy (performed with synchrotron radiation); LEED showed the characteristic splitting of the (1x1) diffracted beams associated with the (23x√3)rect. 'herring-bone' reconstruction. Methylthiolate overlayers were obtained by exposing the surface to a typical exposure of ~10×10^{-6} mbar.s of dimethyldisulphide ($(CH_3S)_2$). Initial tests of the dosing procedure confirmed that this led to a LEED pattern characteristic of the (√3x√3)R30º phase, but a significant deterioration of the diffracted beam intensities with time over a period of a few minutes indicated a substantial degree of electron-beam radiation damage. This type of damage can be reduced by the use of channel-plate amplification of the diffraction pattern in a low-current (~nA) LEED optics, but it is characteristic of the standard optics used in these experiments with higher (~μA) incident currents. For the NEXAFS measurements LEED patterns to check the surface phase were therefore recorded only after collecting these spectra. At room temperature the intense monochromated undulator radiation on the ESRF beamline also led to significant modification of the thiolate layer, characterised by pronounced changes in the S 1s photoemission spectrum over a period of a few tens of minutes, with new chemically-shifted components appearing. Cooling the sample to 160 K prior to exposure to the synchrotron radiation greatly reduced this problem, with no detectable change in the S 1s photoemission spectrum over a period of ~1 hour required to record 1-2 NEXAFS spectra, a finding consistent with an earlier more detailed investigation of radiation damage in thiolate layers on gold [15]. As an added precaution, however, the sample position was adjusted at regular intervals between spectral measurements to ensure that all data were taken from regions of the surface that had received no more than ~1 hour of radiation exposure. Further characterisation of the surface phase was obtained from S 1s NIXSW [16] measurements in the (111) and $(\bar{1}11)$ conditions, which confirmed that the associated structural parameter values (the coherent position and the coherent fraction) were consistent with those obtained in previous studies. In addition, C 1s NIXSW measurements were made in both of these geometries, providing entirely new information described below.

In general NEXAFS data can be obtained through a number of different detection modes that all track the refilling of the core hole created, namely X-ray fluorescence, Auger electron emission, or total (or partial) electron yield [13]. All of these methods are potentially challenging for the particular case of S-containing species on Au surfaces due to the many core levels of Au and their specific energies. In particular, at the S K-edge the photon energy (~2470 eV) is sufficiently close to the Au M_{IV} and M_V edges (2291 eV and 2206 eV) to ensure a high Au 3*d* photoionisation cross-section, leading to strong substrate fluorescence and photoelectron signals, together with a high background of inelastically-scattered and secondary electrons. Attempts to make the measurements by S K_α fluorescence, or by measurements of partial or total electron yields, failed to detect any significant change in signal at the S K-edge due to the very poor signal-to-background ratio. The same difficulty was found in trying to identify and use any S Auger transition associated with direct refilling of the S K-shell hole. The one method that proved successful, albeit with relatively poor signal-to-background ratio, was to monitor the intensity of the S LVV Auger peaks at a kinetic energy of ~150 eV. This emission arises in part from L-shell holes created in the Auger cascade processes involved in refilling the S K-shell hole (a process that monitors the initial S K-shell ionisation). However, the dominant contribution is from L-shell ionisation by secondary and inelastically-scattered electrons, most of which are associated with Au photoionisation, although a small fraction of these also derive from S photoelectron and S K-shell Auger electron emissions. The NEXAFS spectra presented here were therefore measured by recording a low-resolution spectrum of this S LVV Auger peak at each photon energy, and then summing the intensities within each such spectrum; background subtraction was achieved by subtracting a smoothed version of the photon-energy dependence of a similar measurement of the electron emission intensity 10 eV higher in kinetic energy. These NEXAFS spectra were recorded in a series of incidence directions from normal to 10° grazing, corresponding to angles of the polarisation vector, **A**, relative to the surface normal, θ_p, from 90° to 10°, for several different surface preparations.

To extract structural and electronic information, S K-edge X-ray absorption spectra were simulated in the StoBe code [17] for different structural models. Adsorption of thiolate on the clean Cu(100) and Au(111) surfaces was modelled based on cluster models with 25 metal atoms, together with the adsorbate comprising either methylthiolate alone or a combination of methylthiolate and Au adatoms. The theoretical calculations were based on density functional theory on the level of gradient-corrected exchange and correlation functionals [18, 19]. All models were geometry optimised, with the metal atoms in the underlying surface constrained to their bulk positions, before extracting the electronic information.

For hydrogen, carbon and sulphur, triple-zeta valence basis sets including polarisation functions (311/1), (7111/411/1) and (73111/6111/1) were used [20]. For copper a double-zeta valence basis set (63321/5211*/311+) was used [21]. Effective core potentials were used for gold [21]. For accurate spectral simulations, the core-excited sulfur was described using the core extended IGLO-III basis set of Kutzelnigg *et al.* [22] which allows for core relaxation effects. The theoretical x-ray absorption spectra were calculated in the half core-hole transition potential approximation [23] in combination with a double-basis set procedure [24, 25] where, after convergence, the basis set was augmented with a large, diffuse basis set to better describe Rydberg and continuum states. The energy scale of the simulated spectra is corrected with ΔKohn-Sham calculations [25] of the total energy differences between the core-excited states and the electronic ground state.

For direct comparison with the experimental spectra, the discrete calculated spectra were convoluted using Gaussian functions of constant full-width-at-half-maximum (fwhm) of 2.0 eV below 2465.0 eV, linearly increasing up to 11 eV at 2495 eV in order to correct for the approximate description of the continuum wavefunctions by diffuse localised basis functions. Constant shifts of the absolute energy scale were also applied for the theory/experiment comparison as described in the following section.

The mode of data collection and analysis for the NIXSW was as described in more detail in earlier publications (e.g. [7, 8, 16]). Specifically, measurements were made at normal incidence to both the (111) and $(\bar{1}11)$ scatterer planes, monitoring the absorption at the S and C atoms by measuring the photoelectron energy distribution curves (EDCs) around the S 1s and C 1s peaks as the photon energy was stepped, in 0.2 eV increments, through the XSW energy range. Each of these EDCs was then fitted to a peak and a background, and the variation of the area of each peak as a function of photon energy was normalised to give the XSW absorption profiles. As may be expected, the cross-section for photoionisation of the C 1s state is low at the relatively high photon energies associated with the {111} NIXSW conditions, so the signal-to-background ratio is poor in the C 1s EDCs. Nevertheless, this same basic procedure led to acceptable NIXSW absorption profiles. These absorption profiles were fitted by the standard XSW formula, corrected for the non-dipole effects in the photoemission [16], to obtain the two key structural parameters for each profile, namely the coherent position, d_H and the coherent fraction, f_H, for each set of (hkl) reflections denoted by H.

3. NEXAFS results and discussion

A representative set of the raw S K-edge NEXAFS spectra from the Au(111)(√3x√3)R30°-CH_3S surface, with no further modification other than background subtraction as described above, is shown in Fig. 1. Despite the relatively high noise level, the main trends are clear. Specifically, the spectra are dominated by two features at nominal energies of 2469.6 eV and 2472.5 eV. The lower energy feature has its highest intensity with the polarisation vector nearly normal to the surface (θ_p=10°) and has a very low (possibly zero) intensity when the polarisation vector is parallel to the surface (θ_p=90°) . The higher energy feature has a weaker polarisation-angle dependence, but appears to be more intense with the polarisation vector parallel to the surface.

As remarked above, NEXAFS spectra of molecular adsorbates are most commonly interpreted entirely in terms of intramolecular resonances, and in the case of alkylthiolates on other surfaces this typically involves identifying a single spectral feature as due to excitation to a S-C σ* resonance. Fig. 2 shows, as an example, spectra [26] recorded at grazing and normal incidence from methylthiolate adsorbed on Cu(100) on which the structure is known: surface EXAFS [27] and NIXSW [26] studies show the S headgroup atom to occupy the four-fold coordinated hollow sites (Fig. 3). In this earlier work the dominant peak at grazing incidence labelled 'B' was interpreted as the S-C σ* resonance, and the fact that it is intense at grazing incidence and weak (or absent) at normal incidence was taken to imply that the S-C bond direction was near-normal to the surface; excitations to a σ-symmetry final state are expected to show an intensity which varies as $\cos^2\theta_A$, where θ_A is the angle between the polarisation **A**-vector of the incident radiation and the σ-symmetry axis, in this case along the S-C bond direction. By contrast to these data on Cu(100) (which are very similar to those for methylthiolate on Cu(111) [28]), the spectra of Fig. 1 recorded from Au(111) show *two* strong peaks in the near-edge region, so it is far from obvious, *a priori*, which of these corresponds to the intramolecular S-C σ* resonance. The origin of the second peak is also unclear, though the only reasonable interpretation is that it is not intramolecular in origin, but must be related to the surface bonding. As such, this second feature may provide valuable information on the local adsorption geometry.

In order to understand the spectra of Fig. 1, and establish how they may illuminate the surface structure, we have therefore conducted theoretical simulations of the NEXAFS for a series of possible structural models. As a first test of the theoretical approach for adsorbed methylthiolate we have performed calculations for the Cu(100)/methylthiolate system for which the local structure is known. The results are shown in Fig. 2, compared with the (previously published [26]) experimental data. In order to achieve this comparison the photon energy scale of the theoretical calculations has been offset by 5 eV relative to that of the experimental data; in part, this may be attributed to the difficulty of calculating these *absolute* energies accurately, but the absolute experimental energy scale of these old measurements is uncalibrated, and this could also be a source of this discrepancy. The agreement between theory and experiment is rather good. At grazing incidence, the spectra are dominated by two main peaks labelled B and D, whereas at normal incidence there are three peaks, denoted A, B' and C.

From the electronic structure information in the spectral simulations, the features in the X-ray absorption pre-edge range can be described in terms of the mixing of molecular thiolate states with the underlying metal surface. The valence states of thiolate overlap the density of states of the Cu(3d) band, forming bonding and anti-bonding combinations. The S-C bonding and S lone-pair states overlap the lower part of the Cu(3d) band, thereby forming an occupied Cu-S σ bonding band with the coordinating metal atoms. Above the Fermi level, the S-C σ^* anti-bonding and S lone-pair states form a resulting unoccupied Cu-S σ^* anti-bonding band. The B and D peaks are due to the S-C σ^* anti-bonding states, in which the D state has S(d) character. The S lone-pair states give rise to the in-plane A, B' and C states, in which the latter have strong H-C σ^* anti-bonding character.

This comparison of experimental and theoretical spectra leads to two important conclusions: first, the original assignment of the single dominant peak to an intramolecular S-C σ* resonance is basically correct, but second, it is possible to understand far more detailed features of the spectra through the use of the theoretical calculations. This successful application of our theoretical method to the case of Cu(100)/methylthiolate also gives confidence in our primary interest here, namely application to the same adsorbate on Au(111).

Fig. 4 shows the results of the NEXAFS simulations for three distinct adsorption models of methylthiolate on an unreconstructed Au(111) surface with the S headgroup atom in the 'fcc' three-fold-coordinated hollow site (directly above a third layer Au atom), in a two-fold-coordinated bridging site, and in a one-fold-coordinated atop site. The cluster models used for the calculations are shown in Fig.3. For the theoretical NEXAFS spectra from the Au surface the absolute energy scale has been offset by 9 eV in order to achieve the best agreement with the peak positions of the experimental spectra of Fig. 1. In this case the energy calibration of the experimental data is believed to be reliable, so the discrepancy must be attributed to problems in obtaining the correct absolute energies in the calculations. Comparison of the data for Fig. 4 with the experimental spectra of Fig. 1 shows that only the calculations for the atop structure give the qualitative behaviour seen in the experimental data. For the hollow site the theoretical spectra are quite different from the experimental results. For both the bridge and atop geometries, the theoretical spectra reproduce the qualitative two-peak character of the experimental data, but only the atop structure yields a polarisation angle dependence similar to that of the experimental spectra, with the lower energy peak below 2470 eV almost vanishing with the polarisation vector in the surface plane (θ_p=90º). By contrast, for the bridge site, the intensity of this feature shows only a slight attenuation relative to the size of the edge-jump at (θ_p=90º), quite unlike the behaviour seen in the experimental data.

Fig. 5 shows the results of a similar set of calculations for the two adatom reconstruction models referred to in the introduction; these models are shown at the bottom of Fig. 3. On the left are shown two variations of the model involving adsorption atop an Au adatom occupying one of the two distinct three-fold coordinated hollow sites. In fact the NIXSW data indicate that for methylthiolate the adatoms must occupy only fcc hollow sites, but for longer alkyl chains, both of these sites may be occupied [8]. On the right is shown the Au-adatom-dithiolate model proposed on the basis of STM observations at low thiolate coverage [9]; in this case the Au adatom occupies a bridging site on the surface and two thiolate species are bonded on either side of this adatom such that the S headgroup atoms are in near-atop sites relative to the underlying outermost Au(111) surface layer. All of these models involve the S headgroup atom being atop an Au atom, so the local geometry is somewhat similar to the atop site on the unreconstructed surface. However, in the case of the Au-adatom-dithiolate model, there is a second Au-S bond that is nearly parallel to the surface, so one might expect a rather different behaviour of the NEXAFS in this case. Fig. 5 shows that the NEXAFS for all these adatom models (independent, in the case of the hollow-adatom model, of which hollow is occupied) are rather similar to the spectra from atop adsorption on an unreconstructed surface, and thus also reproduce the main trends of the experimental data.

A key question is the origin of the lower energy peak in all of these spectra. The theoretical calculations show that this is largely of S-Au σ^* character, and also confirm that the higher energy peak corresponds to the intramolecular S-C σ^* resonance. Fig. 6 shows the character of the associated unoccupied molecular orbital final states associated with the low energy peak (excited by out-of-plane radiation – i.e. $\theta_p=0^o$) and the higher energy peak (excited most strongly by in-plane radiation – i.e. $\theta_p=90^o$).

On this basis, one can understand the polarisation-angle dependence of the two spectral peaks. For an exact atop geometry the S-Au bond direction is perpendicular to the surface, and excitation to a σ-character final state should vanish at $\theta_p=90^o$. In fact this feature does not quite vanish in the in-plane calculations, because the small-cluster structurally-optimised model used in the calculations places the S atom slightly off-atop; for the unreconstructed surface there is a tilt of the Au-S bond directions of 11^o, while adsorbed on an Au adatom in a hollow site this tilt angle is 5^o and 3^o for the fcc and hcp adatoms, respectively. The assignment of the higher energy peak to the intramolecular S-C σ^* resonance also allows us to estimate the tilt of the S-C bond relative to the surface normal from the variation of the intensity of this peak with polarisation direction in the experimental spectra. A full quantitative analysis is difficult due to the poor signal-to-noise ratio of the experimental spectra and associated difficulties in defining the true background and the size of the edge-jump, but it is clear that this feature has a significant intensity at all measured polarisation angles, so the bond direction can be neither perpendicular nor parallel to the surface. This peak intensity would actually be expected to show *no* variation with polarisation direction if the bond were to be tilted by the 'magic angle' of 54.7º. In fact the spectra of Fig. 1 indicate that the intensity of this resonance is somewhat larger at normal incidence, indicating that the S-C bond is probably tilted from the surface normal by somewhat more than this 'magic' angle, perhaps to a value of ~60°.

The conclusion, based on the comparison of the experimental spectra with the theoretical calculations of Figs. 4 and 5, that the local adsorption geometry is atop, is consistent with the conclusions of the earlier photoelectron diffraction [6] and NIXSW [7] studies. The remaining question, of course, is whether NEXAFS allows us to distinguish the different local atop models, namely atop an unreconstructed surface, or in one of the Au adatom models. In this regard, one surprising result of the calculations is that the calculated NEXAFS spectra for the Au-adatom-dithiolate are very similar to the pure atop structures, and also consistent with the experimental results. Superficially, at least, there seems to be no influence of the additional Au-S bond that is nearly parallel to the surface in this moiety, but is absent in the hollow-adatom and unreconstructed atop models.

The reason for this surprising result may be understood from the data of Fig. 7. In the upper part of the figure is shown the simulation for the Au-adatom-dithiolate model of the in-plane excitation summing over all azimuths (as in the experiment on a three-fold symmetric surface); this curve, marked 'total in-plane', is the same as that shown in Fig. 5. Below this 'total in-plane' spectrum are the individual components corresponding to excitation with the polarisation vector in the surface plane but in different azimuthal directions: specifically along (*x*), and perpendicular to (*y*), the S-Au(adatom)-S bonding direction. Perpendicular to the S-Au-S axis the spectrum is dominated by the S-C σ* resonance (at ~2473 eV). Along the S-Au-S axis there is the expected in-plane S-Au σ* resonance which is seen to dominate the spectrum. However, the energy of this σ* resonance associated with the S-Au(adatom) bonding parallel to the surface (~2472 eV) is very close to that of the S-C σ* resonance, and this occurs at an energy that is very significantly higher than that of the excitation into the S-Au σ* orbital perpendicular to the surface (~2469 eV), due to bonding to the Au atom directly below the S atom. At the bottom of Fig. 7 is shown the theoretical spectrum for in-plane excitation (together with the azimuthally-resolved component spectra) of a model structure that includes the bridging Au adatom of the dithiolate structure, but contains only one thiolate species. In this case the spectrum *does* show strong intensity in a lower energy peak, and the separate azimuthal components clearly show this intensity to be associated with the S-Au(adatom) bond parallel to the surface. Overall, therefore, these calculations show that the presence of the *two* thiolate species strongly modifies the energy associated with the S-Au σ* orbital parallel to the surface within the dithiolate, making its NEXAFS spectra similar to those of the single Au adatom model. Coincidentally, the overlap of the σ* S-C and σ* S-Au(adatom) NEXAFS features for the dithiolate structure could, if this is the correct structural model, influence our estimate of the S-C bond tilt angle discussed above. However, as shown below, NIXSW data provides an independent measure of this parameter.

We must conclude, therefore, that while this comparison of the experimental and theoretical NEXAFS spectra clearly supports the other experimental evidence that the S headgroup atom of methylthiolate on Au(111) occupies a local atop site, it is unable to distinguish between the different reconstructed and unreconstructed surface models that contain this key ingredient. One minor difference to be seen in the calculated NEXAFS spectra for the three distinct atop structures is the energy separation of the S-Au and S-C σ* resonances; for the thiolate atop an unreconstructed surface, this separation is approximately 4.3 eV, for thiolate atop an Au adatom, 3.9 eV, and in the Au-adatom-dithiolate model, 3.4 eV. This final value is closest to the experimental value of approximately 3.0 eV, but the exact separation of the peaks in the theoretical calculations on these small clusters is probably not sufficiently reliable to allow the preferred model to be distinguished.

4. NIXSW results and discussion

In previous NIXSW studies of this adsorption system only X-ray absorption at the S atoms has been investigated and these results [7] have, as reported above, clearly indicated that the S atoms occupy sites atop Au atoms in bulk continuation sites. This conclusion could be consistent with adsorption atop an unreconstructed surface, atop Au adatoms in fcc hollow sites, or adsorption in the Au-adatoms-dithiolate moieties. Here we present new NIXSW results that not only reproduce the results of the earlier measurements of absorption at the S atoms, but include similar measurements of absorption at the C atoms.

The experimental absorption profiles provided by the S and C 1s photoemission signals as the photon energy is scanned through the (111) and $(\bar{1}11)$ NIXSW conditions are shown in Fig. 8. The theoretical fits shown superimposed on these experimental data are defined by two structural parameter, the coherent position and the coherent fraction, and the associated values of these parameters for each absorber atom in each of the two different reflection geometries [16], are given in Table 1. The values given, and the precision estimates, are based on the results of several different measurements including several surface preparations; the number of measurements of each parameter is given in parentheses after the parameter value. In the case of absorber atoms occupying single high-symmetry adsorption sites, the coherent position provides a measure of the spacing of the absorber atom from the nearest (extended) bulk scatterer plane, and under these conditions the coherent fraction is expected to be high (in the range ~0.8-1.0), any reduction below the ideal value of unity being attributable to a combination of dynamic and static disorder. Lower values of the coherent fraction are generally associated with adsorption in low-symmetry sites, or a multiplicity of sites; some examples of this will be discussed below.

For the S absorbers the values of the two NIXSW parameters for both scattering geometries given here are in excellent agreement with those reported previously. The height of the S atoms above the outermost extended bulk scatterer plane, $z_{(111)}$ is equal to the product $(d_{(111)} + n\ )\ D_{(111)}$, where $D_{(111)}$ is the bulk interlayer spacing of the (111) scatterer planes, and n is an integer. In general only one value of the integer n is consistent with physically realistic bondlengths, and the present case it is clear that the value of n is 1; values of 0 or >1 yield Au-S bondlengths that are implausibly short or long. The resulting value of $z_{(111)}$ is 2.45 Å. Note that this distance is not necessarily the true height of the S atom above the outermost Au atomic layer, as the XSW technique references the atomic positions to the extended bulk lattice [16]; in practice, for an unreconstructed fcc (111) metal surface, the net relaxation of the outermost surface layers is expected to be very small. Moreover, as reported previously [7, 8], the values of $d_{(111)}$ and $d_{(\bar{1}11)}$ obtained from NIXSW experiments on the S atomic absorption triangulate perfectly to an atop geometry. Specifically, for an atop geometry we expect $d_{(\bar{1}11)} = (d_{(111)} + n)\ /3$, giving a value of 0.35, in perfect agreement with the experimental value. For comparison, adsorption in hcp hollows, fcc hollows, or either in bridge sites or having equal occupation of the two distinct hollows, would lead to expected $d_{(\bar{1}11)}$ values of 0.68, 0.02 and 0.85 respectively. As mentioned above, however, this simple triangulation for the high-symmetry single adsorption sites is strictly only applicable if the coherent fractions are reasonably high (≥~0.8). Table 1 shows that $f_{(111)}$ is broadly compatible with this requirement, but $f_{(\bar{1}11)}$ is not. In fact the earlier report of similar measurements also showed a low value of $f_{(\bar{1}11)}$ of 0.65, though the value here is even lower. Its origin is unclear; in part it may be attributed to a large amplitude wagging vibration of the Au-S bond that is perpendicular to the surface; this would lead to significant movement parallel to the surface, and thus perpendicular to the $(\bar{1}11)$ scatterer planes inclined at 70.5º to the surface. The fact that our new measurements are made at reduced temperature, however, indicates that there must be some contribution from static disorder.

We now turn to the new results for the C atom absorption. Here, too, the only physically reasonable value of n needed to extract $z_{(111)}$ from the coherent positions of Table 1 is also unity. This choice places the C atoms 0.38 x 2.35 Å = 0.89 Å higher above the surface than the S atoms. Taking the S-C bondlength as 1.82 Å as in methanethiol [27, 29] leads to an implied angle between the S-C bond and the surface normal of 61°, clearly consistent with the interpretation of the NEXAFS spectra. Triangulation leads to the following expected values of $d_{(\bar{1}11)}$ for different local geometries, namely: 0.47 (atop); 0.80 (hcp hollow); 0.14 (fcc hollow); 0.97 (bridge or mixed hollows). Clearly, the triangulation of the d_H values indicates that the C atoms occupy either bridging sites or occupy the two distinct hollow sites with equal probability. In these cases, however, the coherent fraction values are particularly important, because for these two solutions, bridge and mixed hollows, even perfect ordering with no vibrational amplitudes leads to $f_{(\bar{1}11)}$ values of 0.50 and 0.33 respectively. In reality, of course, lower values are to be expected from the experiment.

To understand this issue of triangulation of low-symmetry and mixed sites we consider the expected $(\bar{1}11)$ coherent position and coherent fraction values for an adsorbing atom at some arbitrary lateral position on the surface. The fcc(111) surface has three-fold rotation and mirror symmetry (3mm or C_{3v}), so if the adsorption site has lower symmetry one must take account of occupation of all the symmetrically-equivalent sites, obtained by the application of the substrate symmetry operations, that must be equally probable. One must therefore calculate the NIXSW parameter values for equal occupation of these M symmetrically-equivalent sites, each denoted by an index m. To do so one must first determine, by simple triangulation, the value of $d_{(\bar{1}11)}$ for the mth site, denoted by d_m; assuming perfect static and dynamic order for each site (i.e. $f_{(\bar{1}11)}$=1.0), the resulting coherent fraction and coherent position values, f_{co} and d_H, are then given by

$$f_{co}\exp(2\pi i d_H) = \frac{1}{M}\sum_{m=1}^{M}\exp(2\pi i d_m)$$

Fig 9 shows the contour maps of these two $(\bar{1}11)$ NIXSW parameters as a function of lateral position on the Au(111) surface, assuming the height of the emitter above the surface is independent of the lateral position; the calculations used in this figure also assume that fcc and hcp hollow sites are equally probable, effectively making the surface six-fold symmetric. A fuller discussion of this calculation in the context of adsorption on Ni(111) has been presented elsewhere [30, 31].

The coherent position map of Fig. 9 shows only two grey-scale levels, black and white, corresponding to the only two possible values of $d_{(\bar{1}11)}$ that are found for a given value of $d_{(111)}$ under these circumstances; in the present case, in which $z_{(111)}$=1.42, the two possible values of $d_{(\bar{1}11)}$ are 0.47 and 0.97, shown in the coherent position map of Fig. 9 as black and white, respectively. For a range of positions within ~0.8 Å of the atop sites, the values will triangulate to atop ($d_{(\bar{1}11)}$=0.47); for all other lateral positions, the triangulation will yield values consistent with either bridge or mixed hollow sites ($d_{(\bar{1}11)}$=0.97). Our experimental result for the $(\bar{1}11)$ coherent position therefore indicates that the C atoms must lie within the white regions of this map. The coherent fraction map below shows that the positions on the surface at which the sudden switch between the two coherent position values occurs correspond to values of $f_{(\bar{1}11)}$ of zero. For off-atop sites the coherent fraction increases to its theoretical limit of 1.0 as one moves to the exact atop locations; the atop sites have the full symmetry of the substrate, so no summation over multiple equivalent sites is necessary. Elsewhere in the map, the highest coherent fraction value of 0.50 occurs at the exact hollow sites, while the bridge sites correspond to saddle points in the contours with a coherent fraction value of 0.33.

Superimposed on this coherent fraction map is an arc, drawn about one of the exact atop sites, with a radius of 1.59 Å, the length of the S-C bond projected onto the surface for the S-C bond angle defined by the relative heights of the S and C atoms above the surface. The C atoms must lie somewhere on this arc; notice that *all* points on this arc correspond to the NIXSW triangulation of the coherent position values found in the experiment (i.e. to the white regions of the coherent position map). This projected length of the S-C bond is very close to the lateral separation of the atop and hollow site (1.66 Å) on this surface. Thus, if the S-C bond lies in a <211> azimuth, and the S atom lies exactly atop a surface Au atom, the C atom is almost exactly in the hollow site, and the expected maximum possible value of $f_{(\bar{1}11)}$ is 0.50. By contrast, if the S-C bond lies in a <110> azimuth, the C atom is significantly displaced from the ideal bridging site towards the next atop site, and the maximum possible value of $f_{(\bar{1}11)}$ is, according to the contour map of Fig. 7, approximately 0.25. These values of the coherent fraction assume perfect static and dynamic order; the true experimental values will certainly be lower.

The experimental value of $f_{(\bar{1}11)}$ is 0.23±0.07, but we should also note that $f_{(111)}$ for the C atoms is only 0.48±0.12 while $f_{(\bar{1}11)}$ for the S atom has a low value of 0.45±0.08. $f_{(111)}$ is a measure of the static and dynamic disorder perpendicular to the surface, and rather approximately one may regard $f_{(\bar{1}11)}$ as a similar measure of disorder parallel to the surface. As the thiolate species is bonded to the surface through the S atom, it seems likely that the C atoms should show at least as much lateral disorder as the S atoms, while insofar as the reduced value of $f_{(111)}$ for the C atoms may be due to a large amplitude S-C wagging mode, this will also lead to some dynamic disorder in the C atom position parallel to the surface. Both of these observations lead us to expect that the value of $f_{(\bar{1}11)}$ for the C atoms is likely to be significantly reduced (probably by a factor of ~2 or more) relative to the value to be expected in the ideally-ordered system. On this basis, we may expect C in hollow sites to yield a value of ~0.25 or less, whilst for the off-bridge sites a value of ~0.12 or less might be expected. Comparison with the experimental value thus indicates that the C atoms are much more likely to lie close to hollow sites, with the S-C bond aligned along <211> directions, than in the off-bridge sites with a <110> alignment of the S-C bonds.

Figs. 10(a) and 10(b) show that there is a simple rationale for this preferred azimuthal orientation of the S-C bond, namely that the bonds point to the nearest neighbour adsorbate species in the ordered (√3x√3)R30° structural phase. For adsorption of the S head-group atom atop surface Au atoms in an unreconstructed surface, moreover, there are two distinct possible nearest neighbour directions within such an ordered phase, corresponding to opposing tilts in, for example, the $[\bar{2}11]$ and $[2\bar{1}\bar{1}]$ directions, that lead to the C atoms lying over the two inequivalent hollows sites. These are shown in the (√3x√3)R30° unit meshes of Fig. 10(a) and 10(b), with the C atoms above fcc and hcp hollow sites, respectively. This preferred <211> azimuthal tilt direction is consistent with the early forward-scattering photoelectron diffraction data interpretation of Kondoh *et al.* [6].

While the arguments above, and Figs. 10(a) and 10(b), are based on atop adsorption on an unreconstructed surface, the same conclusions emerge for the model in which the thiolate species adsorb atop Au adatoms in fcc hollow sites. Because these Au adatoms are in bulk continuation sites, this can also be viewed as the same structure as those shown in Figs. 10(a) and 10(b), but with the removal of those outermost-layer Au atoms that are not bonded to the thiolate species. From the point of view of the static structure, a model of one adatom per (√3x√3)R30° unit mesh is equivalent to one with two surface vacancies per unit mesh.

The situation for the Au-adatom-dithiolate model, Fig. 10(c), is different. Strictly, it is impossible to construct an ordered (√3x√3)R30° unit mesh structure with a thiolate coverage of 0.33 ML from these moieties, and one must invoke some kind of disorder to rationalise the involvement of this structural element in this ordered phase [12]. However, in this moiety the azimuthal orientation of the S-C bond is defined by the fact that the S-Au-adatom-S direction is constrained by the model to lie along <211>, and that the C-S-adatom bond angle is approximately 101° [9, 32]. This means the S-C bond is 11° from the <110> azimuth, which places the C atom between the hollow and bridge site, but somewhat closer to the bridge. Based on the contour map of Fig. 7, this suggests that value of $f_{(\bar{1}11)}$, in the absence of static or dynamic disorder, should be in the range 0.30-0.35, a value that is 30-40% less than for the hollow site. In view of the relatively poor precision of the experimental measurement of this parameter, and the doubt surrounding the magnitude of the static and dynamic disorder, formally excluding this model on the basis of the NIXSW data is difficult, but it does seem that the models that place the C atom very close to the hollow sites are much preferred. We should note, incidentally, that a recent DFT study [32] has explored a number of variations in the ordering and conformation of the Au-adatom-dithiolate moiety and concludes that models in which the S-adatom-S axis is bent, and the two thiolates are on the same side of this axis (unlike the original model of Fig. 10(c)), may be energetically preferred, at least in the (2√3x3)rect. ordered phase that occurs in the longer-chain thiolates. These preferred structures place one of the C atoms very close to a bridge site and the second C atom in a site displaced significantly from the hollow towards atop. Both of these sites correspond to significantly lower $f_{(\bar{1}11)}$ values than the hollow sites, and so still offer a less favourable fit to the C NIXSW data presented here.

5. Conclusions

S K-edge NEXAFS data from methylthiolate adsorbed on Au(111) in a (√3x√3)R30° ordered phase show two dominant peaks corresponding to transitions to states of σ symmetry, the higher energy feature being the expected intramolecular S-C resonance, while the lower energy feature is due to an excitation into a local S-Au σ* orbital. This assignment of the spectral features is based on cluster calculations that take account of the nature of the final state, as well as the initial state, in the X-ray absorption. The dependence of the relative intensities of these features on the direction of the polarisation vector of the incident radiation shows clearly that the S head-group atom occupies a local atop site (with the S-Au nearest-neighbour bond approximately perpendicular to the surface), and the S-C bond tilted by ~60° relative to the surface normal.

This atop site attribution does not distinguish between three previously-proposed models, namely atop an unreconstructed surface, atop an Au adatom in a hollow site, or atop an Au atom in the outermost unreconstructed surface but adjacent to a bridging Au adatom on an Au-adatom-dithiolate moiety. The absence of the low-energy NEXAFS feature attributed to the transition to the local S-Au σ* orbital in spectra recorded with the polarisation vector parallel to the surface might suggest that there can be no local S-Au bond parallel to the surface, a conclusion that would exclude the Au-adatom-dithiolate model. However, the theoretical simulations show that the fact that there are two thiolate species bonded to the bridging Au adatom in this moiety causes a shift in energy of the NEXAFS feature associated with the S-Au bond that is near-parallel to the surface, such that it overlaps with the S-C σ* resonance. The consequence is that the simulated NEXAFS spectra for the Au-adatom-dithiolate moiety are very similar to those from the single thiolate species adsorbed atop an Au atom that is either an adatom in a hollow site, or a surface layer atom in an unreconstructed surface. It is therefore not possible, on the basis of the NEXAFS data, to distinguish the different local-atop bonding models.

New C NIXSW data, combined with S NIXSW that reproduce previously-published results, show that the C atoms lies 0.89 Å higher above the surface than the S atom, consistent with a S-C bond angle of 61° relative to the surface normal, a conclusion in broad agreement with the NEXAFS results. Triangulation of the C NIXSW, including consideration of the coherent fraction values, favours a solution in which the C atoms lie close to hollow sites in the underlying surface, consistent with S-C bonds lying in the <211> azimuthal directions that correspond to the nearest-neighbour intermolecular directions of the (√3x√3)R30° ordered phase. This azimuthal direction is not consistent with the expected structure of the Au-adatom-dithiolate model in which the S-C bonds lie ~11° from the <110> azimuth, although variations on the conformation of this moiety could, perhaps, lead to an acceptable agreement with the NIXSW data to within the precision estimates of the measurements.

In conclusion, both the NEXAFS and the NIXSW data provide a clear identification of a local atop adsorption site, confirming the conclusions of earlier studies by photoelectron diffraction and NIXSW. New information is provided on both the polar and azimuthal orientation of the S-C bond, the azimuthal results appearing to favour a model in which intermolecular ordering plays a dominant role, and somewhat disfavouring the model based on local Au-adatom-dithiolate moieties in which the internal conformation is an important factor. The new data do not, however, provide a firm basis for rejecting any of the previously-proposed local atop models based on unreconstructed or Au adatom models, although they give further confirmation that the local adsorption site is not hollow or bridge.

Acknowledgements

The authors are pleased to acknowledge the award of beamtime at the ESRF that made these experiments possible.

Tables

element	$d_{(111)}$	$f_{(111)}$	$d_{(\bar{1}11)}$	$f_{(\bar{1}11)}$
S	0.04±0.01 (*6*)	0.78±0.05 (*6*)	0.35±0.04 (*7*)	0.45±0.08 (*7*)
C	0.42±0.02 (*7*)	0.48±0.12 (*7*)	1.00±0.05 (*6*)	0.23±0.07 (*6*)

Table 1 Summary of the structural parameters obtained from the experimental NIXSW data as shown in Fig. 8.

Figure Captions

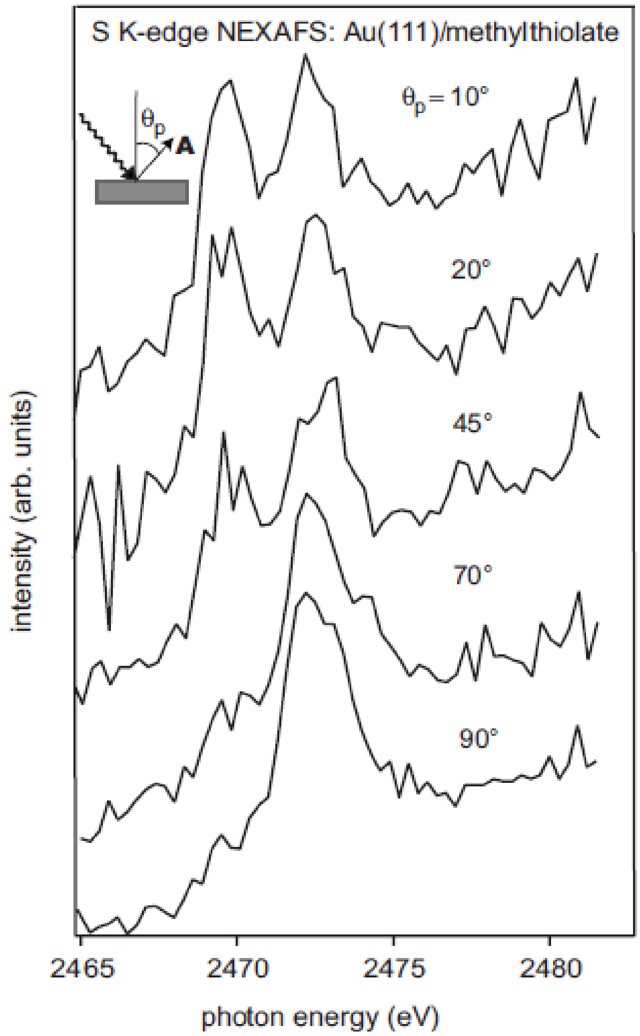

Fig. 1 Experimental S K-edge NEXAFS spectra from the Au(111)(√3x√3)R30°-methylthiolate phase recorded at different value of the angle, θ_p, between the polarisation vector, **A**, of the incident radiation and the surface normal.

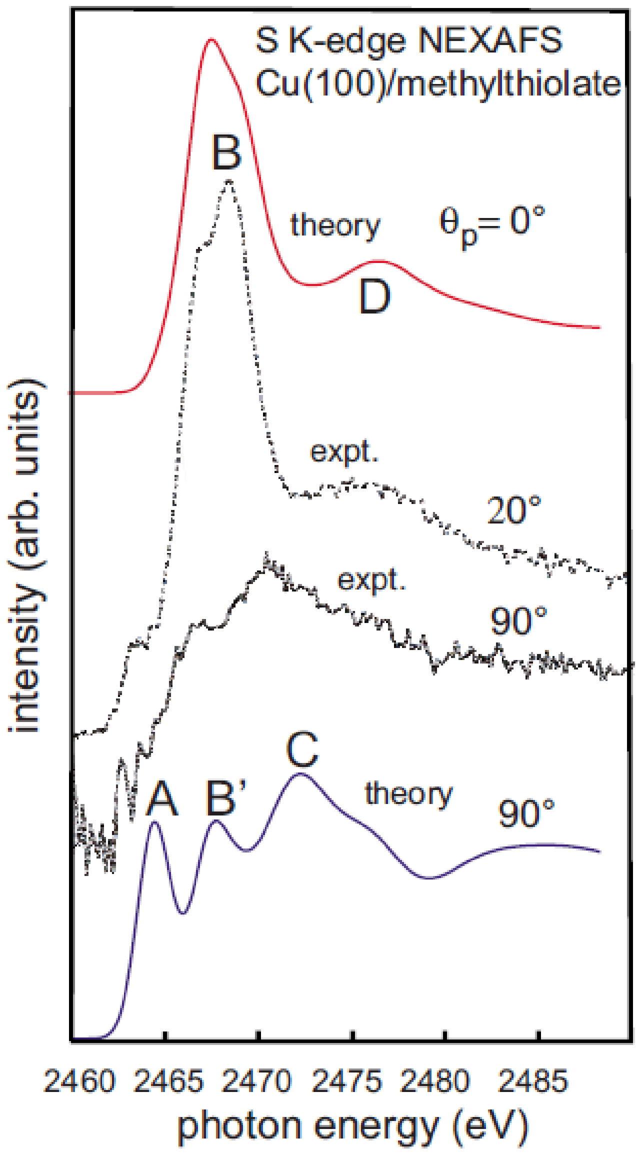

Fig. 2 Comparison of theoretical simulations of the S K-edge NEXAFS spectra from the Cu(100)(2x2)-methylthiolate phase with previously-published [26] experimental spectra. The cluster model (based on the known structure) for these calculations is shown in Fig. 3; see main text for further details of the labelled features in the simulated spectra.

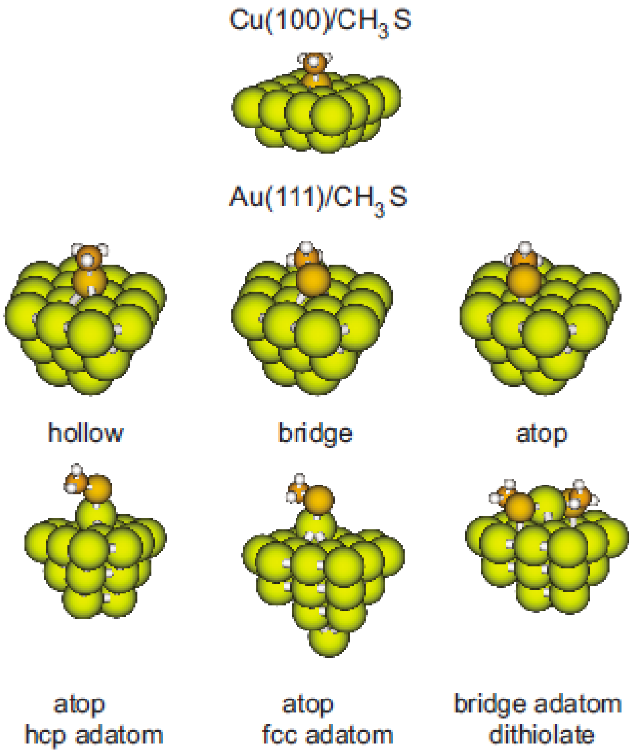

Fig. 3 Schematic diagrams of the clusters for the different surface adsorption models used in the NEXAFS simulations reported here.

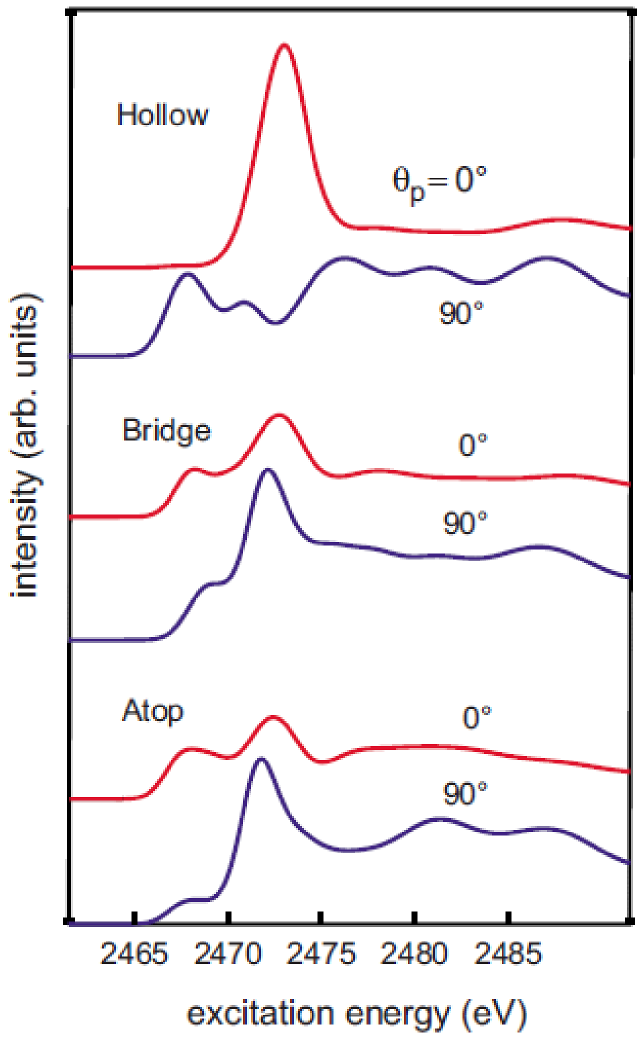

Fig. 4 Theoretical S K-edge NEXAFS spectra from the Au(111)/methylthiolate surface corresponding to the polarisation vector of the incident radiation lying parallel ('in-plane') and perpendicular ('out-of-plane') to the surface (θ_p values of 90° and 0°, respectively) for structural models based on adsorption at different sites on an unreconstructed surface (see middle of Fig. 3).

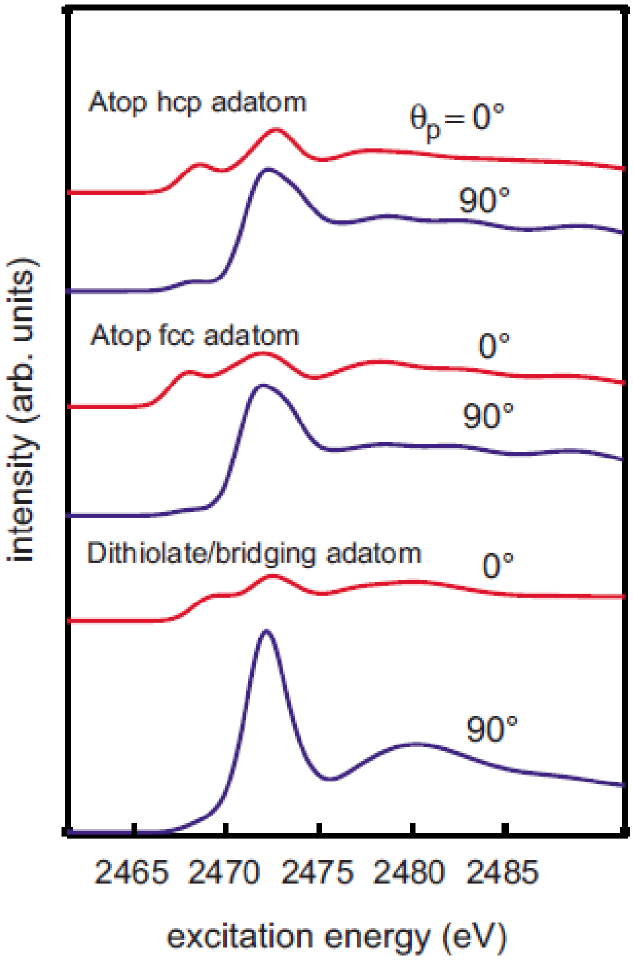

Fig. 5 Theoretical S K-edge NEXAFS spectra from the Au(111)/methylthiolate surface corresponding to the polarisation vector of the incident radiation lying parallel and perpendicular to the surface (θ_p values of 90° and 0°, respectively) for structural models based on different Au adatom reconstruction models (see bottom of Fig. 3).

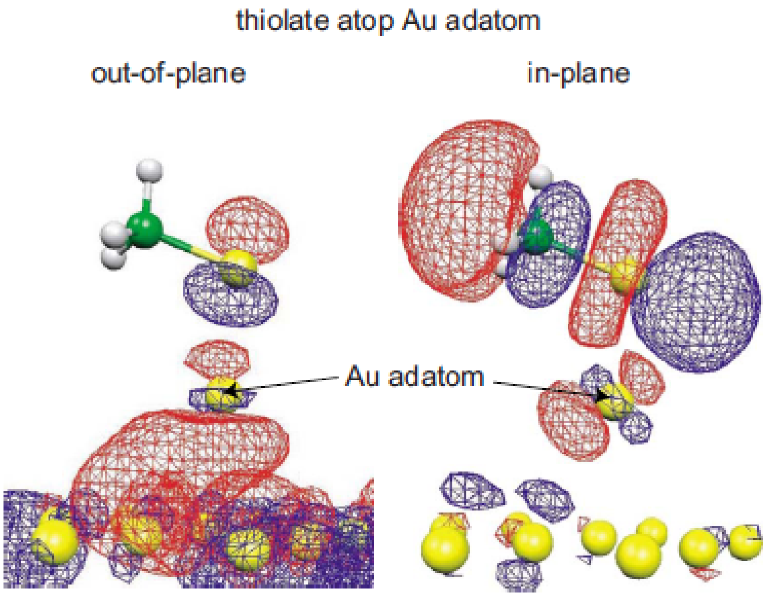

Fig. 6 Representation of the final-state unoccupied molecular orbital states of the low-energy (out-of-plane) and higher-energy (in-plane) peaks in the S K-edge NEXAFS spectra for methylthiolate bonded atop an Au adatom in an fcc hollow site. The figures show iso-amplitude surfaces (red and blue of opposite sign) of the Kohn-Sham orbitals from the transition potential calculations superimposed on a ball model of the thiolate on the surface.

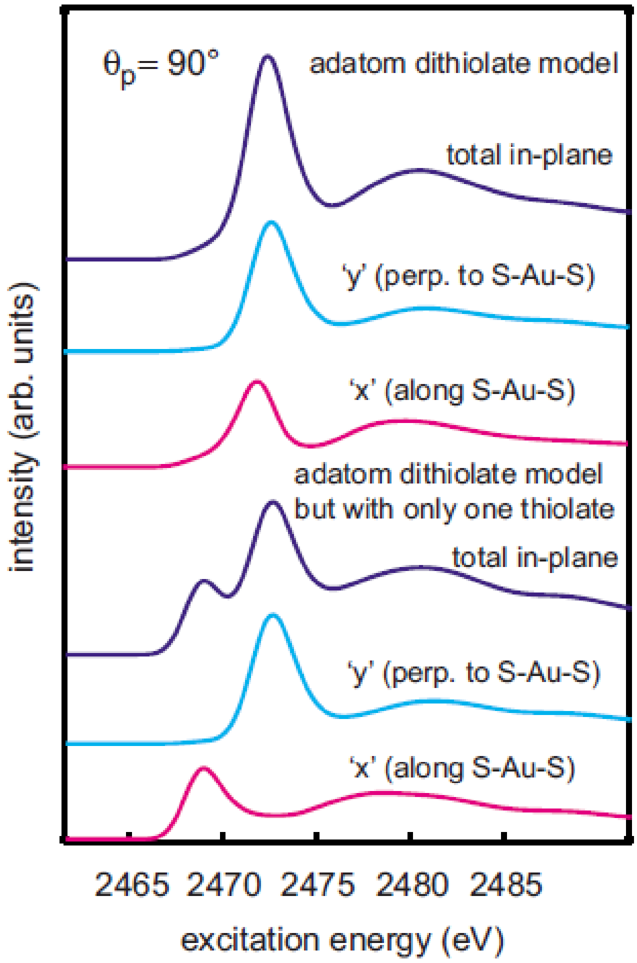

Fig. 7 Theoretical S K-edge NEXAFS spectra from the Au(111)/methylthiolate surface corresponding to the polarisation vector of the incident radiation lying parallel to the surface ('in-plane') for structural models based on the Au-adatom-dithiolate reconstruction model. In addition to the 'total in-plane' absorption, as measured in an experiment at normal incidence, the figure shows the azimuthally-resolved components corresponding the polarisation vector lying parallel and perpendicular to the S-adatom-S axis.

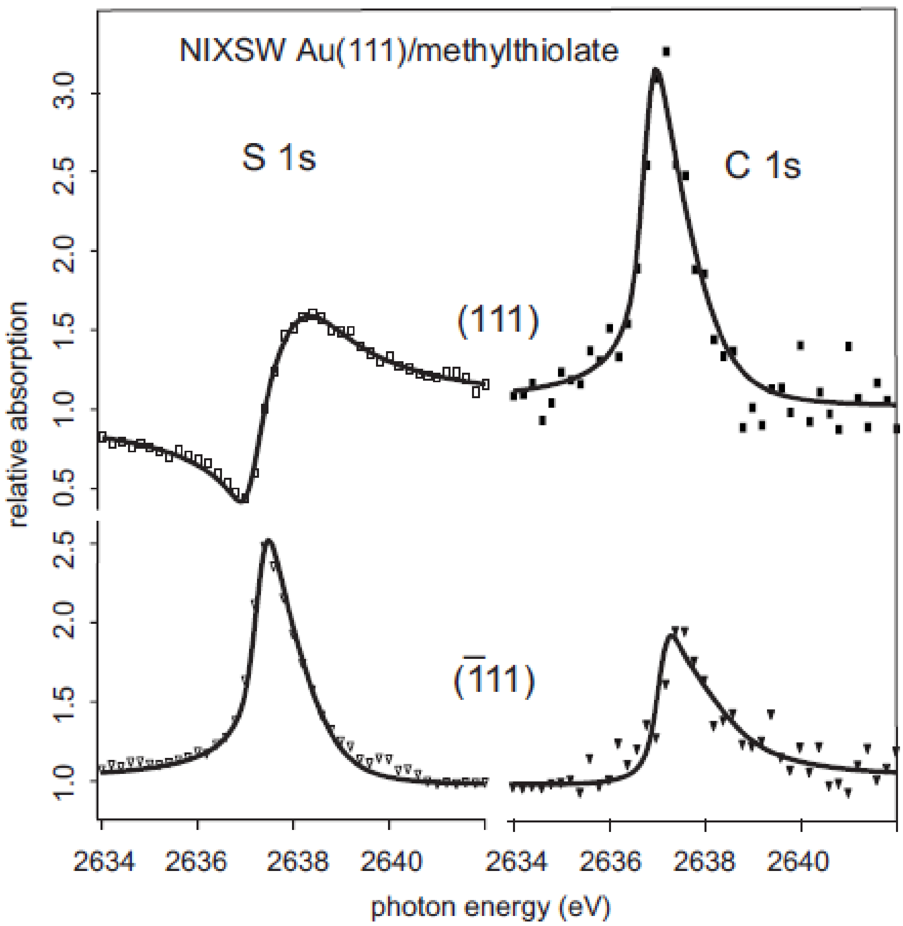

Fig. 8 Examples of individual NIXSW absorption profiles measured at the (111) and ($\bar{1}$11) reflections, by monitoring the S 1s and C 1s photoemission signals, from the Au(111)(√3x√3)R30°-CH_3S surface. The symbols show the experimental data points, the full lines are the theoretical fits.

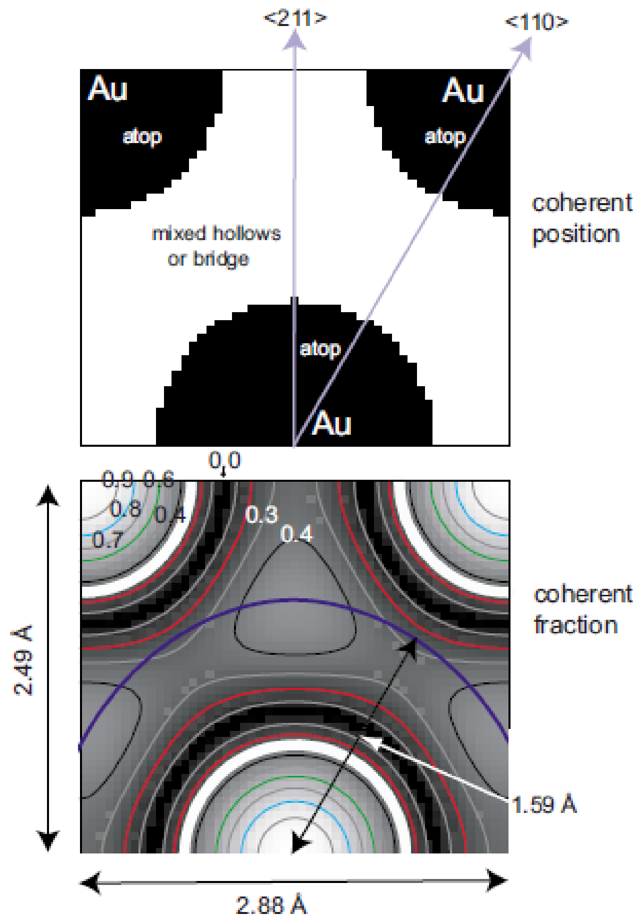

Fig. 9 Contour maps of the $d_{(\bar{1}11)}$ and $f_{(\bar{1}11)}$ values expected for an absorber at different lateral positions on an Au(111) surface and relevant to the interpretation of the C NIXSW data in the present study; a few contour values of the coherent fraction are labelled. The Au surface atoms lie at the centres of the black circular sections in the upper panel. See the text for fuller details.

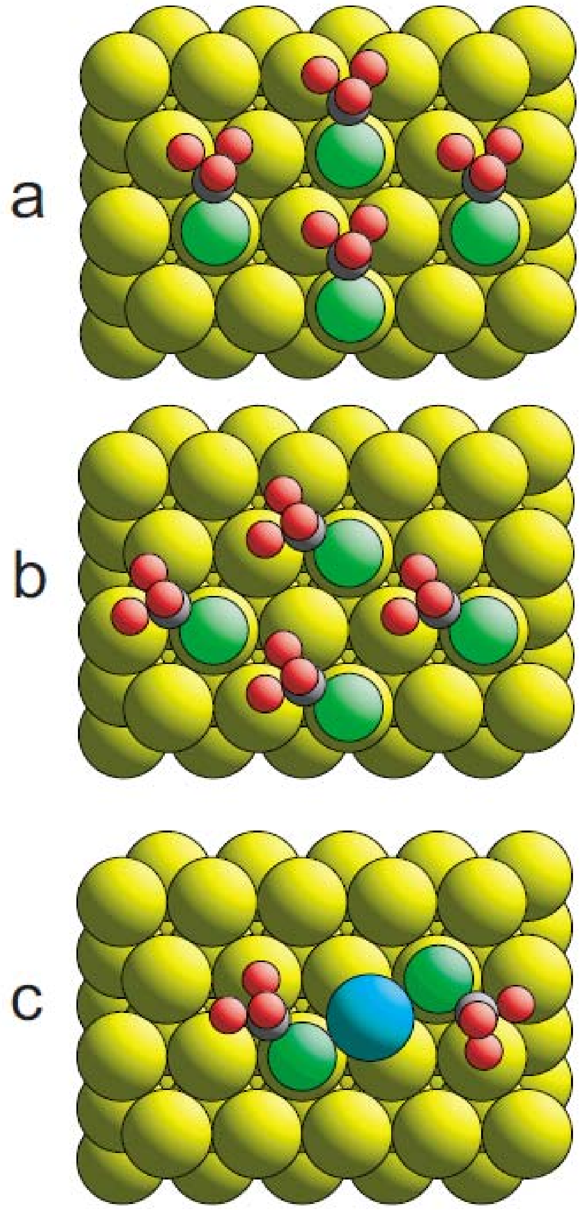

Fig. 10. Schematic plan view of two structural domains (a and b) of the Au(111)(√3x√3)R30°-methylthiolate surface with the S atoms in atop sites on an unreconstructed surface and the C atoms of the methyl group in the two inequivalent hollow sites (fcc in (a)and hcp in (b)), such that the S-C bonds lie in all <211> azimuths. (c) shows a similar schematic plan view of the Au-adatom-dithiolate moiety proposed on the basis of STM images at low coverages of methylthiolate on Au(111) [9]. For clarity the Au adatom in (c) is shown in a different shading from the substrate atoms.

References

1 L. H. Dubois, R. G. Nuzzo, Annu. Rev. Phys. Chem. **43**, 437(1992) .

2 F. Schreiber, Prog. Surf. Sci. **65**, 151 (2000).

3 A. Ulman, Chem. Rev. **96**, 1533 (1996).

4 C. Vericat, M. E. Vela, and R. C. Salvarezza, Phys. Chem. Chem. Phys. **7**, 3258 (2005).

5 D.P.Woodruff, Phys. Chem. Chem. Phys**.** **10**, 7211 (2008).

6 H. Kondoh, M. Iwasaki, T. Shimada, K. Amemiya, T. Yokohama, T. Ohta, M. Shimomura, and K. Kono, Phys. Rev. Lett. **90**, 066102 (2003).

7 M.G. Roper, M.P. Skegg, C.J. Fisher, J.J. Lee, V. R. Dhanak, D.P. Woodruff, and R. G. Jones, Chem. Phys. Lett. **389**, 87 (2004).

8 Miao Yu, N. Bovet, Christopher J. Satterley, S. Bengió, Kevin R. J. Lovelock, P. K. Milligan, Robert G. Jones, D. P. Woodruff, and V. Dhanak**,** Phys. Rev. Lett. **97**, 166102 (2006).

9 P. Maksymovych, D. S. Sorescu, J. T. Yates, Jr. Phys. Rev. Lett. **97**, 146103 (2006).

10 H. Grönbeck and H. Häkkinen, J. Phys. Chem. B, **111**, 3325 (2007).

11 M.L. Molina, and B. Hammer, Chem. Phys. Lett. **360**, 264 (2002).

12 R. Mazzarello, A. Cossaro, A. Verdini, R. Rousseau, L. Casalis, M.F. Danisman, L. Floreano, S. Scandolo, A. Morgante, and G. Scoles, Phys. Rev. Lett., **98**, 016102 (2007).

13 J. Stöhr, *NEXAFS Spectroscopy*, Springer-Verlag, Berlin, 1977.

14 M. Yu, H. Ascolani, G. Zampieri, D.P. Woodruff, C. J. Satterley, R. G. Jones, and V. R. Dhanak, ***J. Phys. Chem. C*** **111**, 10904 (2007).

15 A. Shaporenko, M. Zharnikov, P. Feulner, and D. Menzel, J. Phys.: Condens. Matter **18**, S1677 (2006).

16 D. P. Woodruff, Rep. Prog. Phys. **68**, 743 (2005).

17 K. Hermann, L. G. M. Pettersson, M. E. Casida, C. Daul, A. Goursot, A. Koester, E. Proynov, A. St-Amant, D. R. Salahub, V. Carravetta, A. Duarte, N. Godbout, J. Guan, C. Jamorski, M. Leboeuf, V. Malkin, O. Malkina, M. Nyberg, L. Pedocchi, F. Sim, L. Triguero, and A. Vela, STOBE Software (2002).

18 A. D. Becke, Phys. Rev. A **38**, 3098 (1988).

19 J. P. Perdew, Phys. Rev. B **33**, 8822 (1986); erratum Phys. Rev. B **34**, 7406 (1986).

20 N. Godbout, D.R. Salahub, J. Andzelm, and E. Wimmer Can. J. Chem. **70**, 560 (1992).

21 Basis sets distributed with the Stobe code available under http://www.demon-software.com/public_html/BASIS.html

22 W. Kutzelnigg, U. Fleischer, and M. Schindler, *NMR-Basic Principles and Progress* (Springer Verlag, Heidelberg, 1990).

23 H. Ågren, V. Carravetta, O. Vahtras, and L. G. M. Pettersson, Theo. Chem. Acc. **97**, 14 (1997).

24 L. Triguero, L. G. M. Pettersson, and H. Ågren, Phys. Rev. B **58**, 8097 (1998).

25 C. Kolczewski, R. Püttner, O. Plashkevych, H. Ågren, V. Staemmler, M. Martins, G. Snell, A. S. Schlachter, M. Sant'Anna, G. Kaindl, and L. G. M. Pettersson, J. Chem. Phys. **115**, 6426 (2001).

26 M S Kariapper, C Fisher, D P Woodruff, B C C Cowie, and R G Jones, J. Phys. Condens. Matter. **12**, 2153 (2000).

27 A. Imanishi, S. Takanaka, Y. Yokoyama, Y. Kitajima, and T. Ohta J. Physique Coll. IV **7**, C2 701 (1997).

28 D.L. Seymour, C.F. McConville, M.D. Crapper, D.P. Woodruff, and R.G. Jones *Structure of Surfaces II (Springer Series in Surface Sciences 11)* ed J.F. van der Veen and M.A. Van Hove (Berlin: Springer, 1988) p 189.

29 D.R. Lide, ed. *CRC Handbook of Chemistry and Physics* (CRC Press, Boca Raton, Fl) 2008.

30 G.J. Jackson, J. Ludecke, S.M. Driver, D.P. Woodruff, R.G. Jones, A. Chan, and B.C.C. Cowie Surf. Sci. **389,** 223 (1997).

31 D.P. Woodruff Prog. Surf. Sci. **57**, 1 (1998).

32 G. Grönbeck, H. Häkkinen, and R.L. Whetten, J. Phys. Chem. C **112**, 15940 (2008).